1 **Revision 2**

2 # Cassiterite and Sn mineralization in the giant Bayan Obo

3 # Fe-Nb-REE deposit, North China

4 **Ya-Ting Xu[1], Ru-Cheng Wang[1, *], Mei-Fu Zhou[2], Fu-Yuan Wu[3]**

5 *[1] State Key Laboratory for Mineral Deposits Research, FSC for Critical Earth*

6 *Material Cycling, School of Earth Sciences and Engineering, Nanjing University,*

7 *Nanjing 210023, China*

8 *[2] State Key Laboratory of Ore Deposit Geochemistry, Institute of Geochemistry,*

9 *Chinese Academy of Sciences, Guiyang 550081, China*

10 *[3] State Key Laboratory of Lithospheric Evolution, Institute of Geology and*

11 *Geophysics, Chinese Academy of Sciences, Beijing 100029, China*

12 **** Corresponding author: E-mail, rcwang@nju.edu.cn***

13

14

15

16

17   **ABSTRACT**

18   Critical rare metal deposits are strategic resources as these metals are significant

19   for high-tech industries. Among the critical rare metals, stannum (Sn) in nature is

20   mostly found in Sn-oxide mineral, cassiterite (SnO_2), and closely associated with

21   granite or pegmatite. Carbonatite and alkaline rocks are more likely to contain huge

22   amounts of critical rare metals, especially REEs and niobium (Nb). We reported

23   abundant cassiterite (SnO_2) and evaluated potential Sn mineralization in the Bayan

24   Obo Fe-Nb-REE deposit in northern China, the largest REE deposit worldwide. In

25   this paper, evidence for the Sn enrichment in a carbonatite-hosted REE deposit is

26   given for the first time.

27   REE-Fe ores are dominantly mined in the Bayan Obo deposit. Disseminated,

28   banded and massive ores contain tens to hundreds ppm Sn and vein-type ores are

29   notably rich in Sn (up to 1500 ppm). Through *in situ* micro-zonation mineralogical

30   analyses, two occurrences of cassiterite and several Sn-rich minerals are identified in

31   these REE-Fe ores. Abundant early-stage nanoscale cassiterite inclusions are present

32   within magnetite grains in banded and massive REE-Fe ores, and ubiquitous late-

33   stage granular cassiterite, Sn-rich rutile, titanite, and bafertisite are present in vein-

34   type REE-Fe ores. Multiple U-Th-Pb dating of monazite and columbite-Mn in

35   association with cassiterite yields peak ages of 425 Ma and 419±18 Ma, respectively,

36   revealing coeval Sn and Nb mineralization. We concluded that Sn was derived from

37   carbonatitic magmas, and the dense distribution of cassiterite inclusions in magnetite

38   marked the pre-enrichment of Sn in the Bayan Obo deposit. Subsequent Early

39   Paleozoic hydrothermal events led to the reactivation and further Sn mineralization.

40   Similar to Nb, Sn was mineralized in the Bayan Obo deposit probably to form

41   economically important resources. Our study highlights the potential of Sn

42   mineralization associated with carbonatite-hosted REE deposits.

43   **Keywords:** critical rare metals; cassiterite; Sn mineralization; Bayan Obo deposit;

44   TEM; geochemical characteristics; U-Th-Pb Dating; SIMS

45   **INTRODUCTION**

46   Stannum (Sn), a versatile and economically significant metal, is vital in modern

47   times. Its applications include traditional uses in soldering and plating and high-tech

48   industries such as electronics and renewable energy. Cassiterite (SnO_2) is the most

49   common Sn oxide mineral and the primary ore mineral for Sn extraction. In nature, Sn

50   mineralization is associated mainly with granites, pegmatites, and related metasomatic

51   and hydrothermal systems (e.g., greisens and quartz veins) (Lehmann, 2021) but rare

52   in other rocks.

53   The mantle-derived carbonatites and carbonatite-related deposits are well known

54   to be the primary sources of the world's rare earth elements (REEs), and alkaline-

55   carbonatite complex-related deposits are rich in niobium (Nb), as well as phosphate

56   (P), iron (Fe), and fluorine (F) (Smith et al. 2015; Simandl and Paradis 2018; Beland

57   and Williams-Jones 2021; Verplanck et al. 2022). However, other critical metals in

58   carbonatites or in carbonatite-hosted deposits are still poorly understood. Whereas

59   REEs and Nb are well studied as enriched in specific carbonatite-hosted deposits,

60   adequate data on the occurrences and mineralization potentials of other critical metals

61   in such deposits are lacking.

62   The Bayan Obo REE-Fe deposit in Inner Mongolia, China, is hosted in

63   carbonatites, where intense magmatic differentiation of carbonatite is deemed to

64   facilitate the great REE accumulation (Yang et al. 2019). Multi-stage superposition of

65   magmatism, hydrothermal alteration, and metamorphism has influenced the

66   distribution and characteristics of minerals within the deposit (Song et al. 2018; Yang

67   et al. 2019; Liu et al. 2020; She et al. 2021). Major mineralization events in the

68   deposit, i.e., Nb mineralization, proceed from magmatic to hydrothermal

69   crystallization (Campbell et al. 2014; Smith et al. 2015; Fan et al. 2016; Liu et al.

70   2020). The immense REE mineralization initially took place at around 1.3 Ga in

71   association with carbonatite magmatism (Yang et al. 2011a; Fan et al. 2014; Yang et

72   al. 2017; Li et al. 2021). In addition, at least two younger magmatic-hydrothermal

73   events at around 430 Ma and 270 Ma subsequently contributed to the mineralization

74   through leaching and reactivation of primary minerals (Yang et al. 2011a, 2017;

75   Campbell et al. 2014; Fan et al. 2014; Ling et al. 2014; Li et al. 2021). Although

76   REEs, especially light rare earth elements (LREEs), niobium, and iron have long been

77   recognized as the prime mining resources in the Bayan Obo deposit, we find another

78   valuable hidden resource within this world-class deposit, Sn mineralization, mainly in

79   the form of cassiterite.

80   This study describes the distribution of cassiterite and other Sn-rich minerals

81   among REE-Fe ores, and reveal the genesis of Sn mineralization in the Bayan Obo

82   deposit. We also report precise ages of monazite and parisite associated with

83   cassiterite. Combining all the dating results, we confirm a link between Sn

84   mineralization and other major mineralization events in the Bayan Obo deposit,

85   indicating a potential for Sn resources. By elucidating the nature of Sn mineralization

86   within the Bayan Obo deposit, this study could enhance the understanding of

87   processes that govern Sn enrichment in similar geological settings, and has practical

88   implications for resource assessment, mining strategies, and the sustainable

89   exploitation of Sn resources in carbonatite-hosted REE deposits.

90   **MATERIALS AND ANALYTICAL METHODS**

91   **Sample collection**

92   Several typical REE-Fe ores from the Bayan Obo deposit have been investigated

93   in detail in this work. All the samples were collected from the Main, East, and West

94   Open Pits (see below). Samples DK19-, DK20-, XK19-, XK20-, 17BY-, ZK1917,

95   ZK1918 and ZK1919 were collected at the bottom of the open pits, and ZK1932 from

96   a drill hole in the Main Open Pit. The hand specimens are representative ore blocks,

97   comprising the disseminated ores, the banded ores, the massive ores and the vein-type

98   ores. Detailed features of hand specimens are shown in Figure 2.

99   **Whole rock trace element analysis**

100   Whole-rock trace element compositions of different types of ore from the Bayan

101   Obo deposit were determined using inductively coupled plasma mass spectrometry

102   (ICPMS) at FocuMS Technology, Nanjing, China and the ALS Laboratory Group,

103   Guangzhou, China. About 40 mg powder was mixed with 0.5 ml 60 wt.% HNO_3 and

104   1.0 ml 40% HF in high-pressure PTFE bombs. These bombs were steel-jacketed and

105   placed in the oven at 195°C for 3 days to ensure complete digestion. After cooling, the

106   bombs were opened, dried down on a hotplate, re-dissolved with 5 ml 15 wt.% HNO_3

107   and 1ml Rh internal standard, then sealed and placed in the oven at 150°C overnight.

108   Aliquot of the digestions (dilution factor 2000) were nebulized into Agilent

109   Technologies 7700x quadrupole ICP-MS (Tokyo, Japan) to determine trace elements.

110   Geochemical reference materials of USGS: basalt (BCR-2, BHVO-2), andesite (AVG-

111   2), rhyolite (RGM-2), granodiorite (GSP-2) were treated as quality control. Measured

112   values of these reference materials were compared with preferred values in GeoReM

113   database (Jochum and Nohl, 2008). Deviation were better than 20% for trace elements

114   between 0.5 ~ 5 ppm, better than 10% for these between 5 ~ 50 ppm, and better than

115   5% for these exceeded 50 ppm.

116   **EDS-equipped scanning electron microscope investigation of minerals**

117   Textural and petrographic features of samples were investigated by scanning

118   electron microscope (SEM), using the Zeiss Supra55 field emission scanning electron

119   microscope (SEM) equipped with an Oxford energy dispersive spectrometer (EDS)

120   and a Gatan Mono CL^{3+} detector. The mineralogical mapping was acquired using

121   Advanced Mineral Identification and Characterization System (AMICS), using the

122   Zeiss Sigma 300 field emission scanning electron microscope (SEM) with a Bruker

123   XFlash detector at Nanjing University, China. Backscattered electron (BSE) and

124   energy dispersive (EDS) data are collected on an irregular grid below 5 μm point

125   spacing in the vacuum mode. Acceleration voltage of 20 kV and a beam current of 10

126   nA were used during the data acquisition. The individual spectra from points were

127   grouped based on a similarity search algorithm, and areas of coherent BSE and EDS

128   data were merged to produce segments (i.e., mineral grains). Data from each segment

129   were then compared against a classification scheme to identify the mineral and assign

130   its density. The results were plotted as a map showing the distribution of minerals

131   within the sample.

132   **Electron microprobe analyses of minerals**

133   Chemical compositions of minerals were analyzed using the JEOL 8530 field-

134   emission electron microprobe in Nanjing University. Optimized operation conditions

135   were applied: accelerating voltage of 15 kV, beam current of 20 nA, and beam

136   diameter of 2 μm, counting times of 20 seconds on each peak and half time for

137   backgrounds. All data were updated using standard ZAF correction procedures. The

138   ZAF correction compares the sample-to-sample differences in atomic number effects

139   (Z) on incident electrons (including backscattering and blocking principal) as well as

140   absorption (A) and fluorescence (F) effects on X-rays to find the corresponding

141   correction factor, and then converts the X-ray intensity ratio to elemental content.

142   **Transition electron microscope identification of minerals**

143   Magnetite microstructure investigation was carried out with transition electron

144   microscope (TEM), using a FEI Tecnai G2 F30 instrument equipped with a Lorentz

145   lens, a Bruker XFlash detector and a Fischione high-angle annular dark-field

146   (HAADF) detector at Electron Microscopy Center of Lanzhou University (LZU) of

147   China.

148   **Laser Ablation – Inductively Coupled Plasma – Mass Spectrosmeter (LA-ICP-**

149   **MS) analyses**

150   Trace element composition of magnetite, U-Th-Pb ages of monazite and

151   columbite-Mn were determined *in situ* by laser ablation inductively coupled plasma –

152   mass spectrometry (LA-ICP-MS), using a system consisting of ASI RESOlution S-

153   155 193 nm ArF Excimer laser coupled to Thermo Scientific iCAP Qc quadrupole

154   ICP-MS at the State Key Laboratory for Mineral Deposits Research at Nanjing

155   University of China. The trace element analyses were obtained using a laser beam

156   diameter of 43 μm, maximum energy density of 100 mJ and ablation rate of 4 Hz. The

157   dating analyses were obtained from polished sections using a laser beam diameter of

158   19 μm, maximum energy density of 75 mJ and ablation rate of 3 Hz.

159   **Secondary ion mass spectrometry (SIMS) analyses of U-Th-Pb dating**

160   *In situ* monazite and parisite U-Th-Pb dating was conducted by secondary ion

161   mass spectrometry (SIMS), using a Cameca IMS-1280 instrument at Nanjing

162   University, China. The sample mounts were coated with about 30 nm of high-purity

163   gold to reach < 20 Ω resistance. Positive secondary ions were extracted with a 10 kV

164   potential. Sample charging effects were minimized by optimizing the energy offset to

165   maximum transmission in a 60 eV energy window at the start of each analysis, using

166   the Th^+ and Y_2O^+ as reference peaks for monazite and parisite, respectively. The size

167   of the ellipsoid analyzed spot was 15 μm × 10 μm. The monazite U-Th-Pb analyses

168   calibrated against RW-1 standard ($^{207}Pb/^{235}U$ age = 904.15 ± 0.26 Ma [2σ], Th = 11.8

169   ± 1.0 wt.% [2σ], and Th/U = 42.5 ± 3.0 [2σ]). Monazite MAD and M6 were employed

170   as secondary standards. Parisite grains were mounted together with standard Nist-610

171   and K-9 for accuracy monitoring. A repeatability of 1.5% (1σ RSD) was derived from

172   the measurement of standards. Detailed analytical procedures are the same as those

173   described in (Li et al. 2013) and (Li et al. 2020).

174   **DEPOSIT GEOLOGY**

175   The Bayan Obo REE-Nb-Fe deposit is located at the northern margin of the

176   North China Craton, south of the Central Asian Orogenic Belt (Yang et al. 2011b),

177   about 150 km north of Baotou City in northern China. The deposit is hosted by rocks

178   of Paleo- to Mesoproterozoic Bayan Obo Group, which is unconformably underlain

179   by a basement complex of the North China Craton (Zhu et al. 2015; Fan et al. 2016a).

180   Proterozoic carbonatite dikes, Permian gabbroic, and granitic plutons are widespread

181   (LeBas et al. 1992; Yang et al. 2011a, 2011b; Ling et al. 2014; Zhang et al. 2017). The

182   H8 dolomite unit confined to the south of the Kuangou anticline hosts the majority of

183   orebodies. A narrow ore belt, with an area of ~ 48 km^2, lies in the east–west direction

184   (about 18 km long and 2 ~ 3 km wide). Several REE-Fe orebodies varying in size

185   have been recognized throughout this area, among which are the three largest

186   orebodies, i.e., the Main, East and West Orebodies, being located in the central part of

187   the ore-bearing belt (Fig. 1). Iron ores are the primary commodities from orebodies,

188   followed by REE-Fe ores, REE ores and dolomites.

189   **RESULTS**

190   **REE-Fe ore types and mineral assemblages**

191   The giant Bayan Obo deposit was formed through multi-stage mineralization.

192   Consequently, REE-Fe ores have complex textures and mineral assemblages (Table

193   1). REE-Fe ores can be classified into four main types, namely disseminated, banded,

194   massive, and vein-type ores (Fig. 2). Generally, disseminated ores formed slightly

195   earlier than other types. The disseminated ores occur in the orebodies diffusely, and

196   are mainly composed of dolomite, with minor presences of evenly distributed

197   magnetite, fluorite, bastnaesite and monazite (Fig. 2a, e). Banded ores are composed

198   of alternating bands of deep purple fluorite, magnetite, greenish aegirine, and yellow

199   bastnaesite (Fig. 2b). These bands are thin and narrow in hand specimens, usually less

200   than one centimeter in width (Fig. 2b, f). Massive ores are dominantly composed of

201   magnetite, minor fluorite and aegirine, and a few variably distributed REE minerals

202   (Fig. 2c, g). The vein-type ores are usually formed later than other types, sometimes

203   penetrate or crosscut other types of ores, and are more complex in mineral

204   assemblages of fluorite, calcite, apatite, aegirine and so on (Fig. 2d, h).

205   **Sn concentrations of REE-Fe ores**

206   Whole-rock chemical analyses of REE-Fe ore samples from the Bayan Obo

207   deposit were carried out by ICP-MS, and the full dataset is available in the Appendix.

208   Table A1. Sn contents of the ores are positively correlated with the Nb contents (Fig.

209   3a), but are not strongly correlated with REE contents, such as La (Fig. 3c). Stannum

210   is particularly enriched in late-formed vein-type ores (Fig. 3b, d). Disseminated ores

211   contain the lowest Sn (9 ~ 27 ppm, average of 15 ppm), and banded ores have overall

212   higher Sn contents ranging from 13 to 151 ppm, with an average of 62 ppm. Sn

213   contents in massive ores are variable from 17 to 200 ppm, with an average of 62 ppm.

214   One massive ore (ZK1918) composed of magnetite, aegirine, fluorite and calcite has

215   200.21 ppm Sn. Notably, the aegirine veins contain over 200 ppm Sn and those with

216   numerous bafertisite grains (DK2003) contain the highest Sn up to 1515 ppm among

217   all the analyzed samples in this study (Table 1).

218   **Mineralogy**

219   *Magnetite associated with cassiterite*

220   Magnetite is the main ore mineral in REE-Fe ores, particularly in massive ores.

221   Although cassiterite is rarely reported in carbonatites in literature, magnetite with the

222   appearance of nano to micron-sized cassiterite inclusions is commonly observed in

223   the Bayan Obo REE-Fe ores (Fig. 4a), which is an exotic feature that is worth further

224   studying. Through high-resolution backscattered electronic observation, we

225   recognized some porous domains of magnetite grains in massive ores. Moreover,

226   cassiterite grains included in these porous domains tends to be more than 10 μm in

227   size, distinctly larger than that occurring in relatively intact domains of the same

228   magnetite grains (Fig. 6c). This feature suggests that these magnetite grains

229   underwent hydrothermal alteration and the hydrothermal activities promoted Sn

230   enrichment. As a different occurrence, magnetite may also be observed as small

231   discrete euhedral crystals with well-developed {111} faces in association with

232   clustered cassiterite (Fig. 4c) in vein-type ores of late stage.

233   EPMA results indicate slight variations in chemical compositions between

234   granular magnetite aggregates (massive magnetite) and discrete magnetite grains (Fig.

235   5). LA ICP-MS analyses show that massive magnetite grains with no mineral

236   inclusions have Sn contents of only tens ppm (below 30 ppm), confirming the Sn

237   depletion in this type of magnetite (Table A2). Small discrete magnetite grains exhibt

238   slightly higher Sn (0.07 ~ 0.23 wt.%), Ti (0.40 ~ 1.29 wt.%), and Ca (0.24 ~ 1.37

239   wt.%) and lower Mn than the dominant massive magnetite grains (0.06 ~ 0.16 wt.%

240   Mn) (Table A3). Changes in trace element contents of the two magnetites also reflect

241   further Sn enrichment in the later mineralization process.

242   ***Cassiterite***

243   Cassiterite (SnO_2) is the most common and economically important Sn-bearing

244   ore mineral in nature. In this study, cassiterite, usually in two forms, is widely present

245   in massive and vein-type REE-Fe ores from the Bayan Obo deposit. One is micron-

246   sized cassiterite inclusions dispersed within magnetite grains, and the other is tens of

247   micron-sized clusters associated with hydrothermal minerals veins consisting of

248   fluorite, apatite, calcite, or aegirine (Fig. 6).

249   Across all REE-Fe ore types, cassiterite inclusions in magnetite are anhedral and

250   less than one micrometer; they occur sporadically in some magnetite grains from

251   disseminated ores but are abundant within magnetite grains from massive and banded

252   ores (Fig. 6a-c). Nb-bearing ilmenite or Sn-bearing rutile are also occasionally

253   identified near cassiterite inclusions (Fig. 4a). At least 75 micro-grains of cassiterite

254   (smaller than 1μm) without clear orientation are counted in a small area of about 0.05

255   mm^2 within the massive magnetite from the sample ZK1918 (Fig. 6b). Further TEM

256   study was conducted on ion milling system-assisted foils of magnetite with cassiterite

257   inclusions and, from the perspective of crystal structure, confirmed the existence of

258   tiny cassiterite. HRTEM imaging identified local crystal orientations notably with *d*-

259   spacings of 2.654 Å (101), 2.366 Å (200), 1.672 Å (220) and 2.308 Å (111) for

260   cassiterite, and *d*-spacing of 2.709 Å (104) for ilmenite, respectively (Fig. 4b). In

261   addition, the fast Fourier transform (FFT) image indicated the crystalline cassiterite.

262   Lattice fringe images in the contact area of cassiterite and magnetite show a gradual

263   transition, indicating simultaneous formation rather than later mechanical mixing

264   (Fig. 4d). Dense cassiterite inclusions formed at the same time as massive magnetite

265   mark the pre-enrichment stage of Sn mineralization.

266   Granular cassiterite in banded, massive, and vein-type ores typically occurs as

267   clusters from tens to hundreds of microns in size (Fig. 6a, d, e). These clustered

268   cassiterite grains are closely associated with aegirine, amphibole, fluorite, or calcite,

269   and together form veinlets with variable mineral assemblages that crosscut the

270   magnetite grains. In this case, the individual cassiterite grains are subhedral, tens of

271   microns in size, and closely coexisting with other REE-Nb minerals (commonly

272   bastnaesite, monazite, columbite, and pyrochlore). Clustered cassiterite grains may

273   also densely accumulate in association with Fe-Ti oxides (ilmenite and rutile) (Fig.

274   7a, b). The zoned internal texture of cassiterite grains is revealed by

275   cathodoluminescence (CL) imaging (Fig. 8). As shown in Table 2 (compiled in Table

276   A4), clustered cassiterite grains usually contain trace amounts of Ti, Nb, Fe and Mn.

277   In the Nb + Ta vs Fe + Mn diagram (Fig. 8), all these cassiterite grains are vertically

278   scattered on the left side with higher Fe + Mn than Nb + Ta, plotting within the field

279   of hydrothermal origin. The genesis of clustered cassiterite indicates the promotion of

280   Sn enrichment by hydrothermal activities in the Bayan Obo deposit.

281   ***Sn-rich rutile***

282   Nb-rich variety of rutile (TiO_2), or sometimes ilmenorutile [$(Ti,Nb,Fe)O_2$], has a

283   widespread occurrence in REE-Fe ores from the Bayan Obo deposit. In massive ores,

284   rutile may occur as subhedral crystal aggregates of about 100 μm, coexisting with tiny

285   cassiterite grains (Fig. 7a, b). In vein-type ores, several veinlets of rutile, tens of

286   microns wide and several millimeters long, can be observed in penetrating aegirine

287   grains (Fig. 7c). Sn may substitute for Ti, Fe or Nb in the mineral composition.

288   Chemically, rutile may contain up to 3.36 wt.% SnO_2 (0.30 ~ 3.36 wt.% SnO_2, Table

289   A5-1) and ilmenorutile contains SnO_2 as high as 6.58 wt.% (2.65 ~ 6.58 wt.%, Table

290   A5-2).

291   ***Sn-rich titanite***

292   Titanite, $CaTi(SiO_4)O$, usually appears around Sn-bearing ilmenite in vein-type

293   ores and sometimes shows a zoning texture characterized by alternating brighter and

294   darker strings. Single titanites are variable in SnO_2, and the brightness corresponds

295   well with SnO_2 concentrations: the brighter zones have 9.70 ~ 10.69 wt.% SnO_2,

296   much higher than that of the darker area (0.69 ~ 2.93 wt.%) (Fig. 7d, Table A6). The

297   ion radius of Sn^{2+} ion is close to that of Ca^{2+}, so substitution of homomorphism is

298   obvious among titanite.

299   ***Sn-rich bafertisite***

300   Bafertisite, ideally $Ba_2Fe^{2+}_4Ti_2(Si_2O_7)_2O_2(OH)_2F_2$, is an important Sn-rich

301   mineral phase typifying the vein-type ores. It may occur as narrow veinlets only

302   below 300 microns wide but extending to tens of centimeters long (Fig. 7e) and

303   typically coexists with other Ba-bearing minerals such as baryte, baotite, and

304   cordylite. Bafertisite also appears as fibrous aggregates (Fig. 7f). Sn^{2+} will substitute

305   for divalent iron (Fe^{2+}) in the mineral composition. This mineral generally contains

306   moderate Sn exceeding 2 wt.% (2.70 ~ 4.40 wt.% SnO_2), and fiber bafertisite is much

307   richer in Sn with up to 16.68 wt.% SnO_2 (9.80 ~ 16.68 wt.%), approaching a Sn-

308   analogue of bafertisite (Table A7).

309   **Constraints on the timing of Sn mineralization**

310   Cassiterite grains observed in Bayan Obo are too small to be *in situ* dated with

311   LA-ICP-MS or SIMS techniques. Instead, their coexisting and cogenetic REE

312   minerals (monazite and parasite) from vein-type ores (Fig 9), and Nb mineral

313   (columbite-Mn) from massive ores were subjected to geochronological work on Sn

314   mineralization in the Bayan Obo deposit (Fig. 10).

315   Th-Pb ages tested on thirty monazite grains by LA-ICP-MS range from 375 to

316   663 Ma (Fig. 10a, Table A8). This mineral, co-existing with cassiterite, was also

317   targeted for SIMS dating, yielding an age spectrum of 281 ~ 932 Ma (Fig. 10c, Table

318   A9). Modeled by frequency distribution plot, the monazite ages obtained by the two

319   methods gave the same peak age of 425 Ma (Fig. 10b, d). *In situ* LA-ICP-MS dating

320   for thirteen large grains of columbite-Mn associated with cassiterite, directly analyzed

321   on thin sections, yielded a similar lower-intercept age of 419 ± 18 Ma (Fig. 10e, Table

322   A10) and a weighted average age of 426 ± 26 Ma (Fig. 10f). Besides, another younger

323   peak age of 275 Ma was also obtained by SIMS dating on fifty parisite grains (Fig.

324   10g, h, Table A11). The dating results denote the connection between Sn enrichment

325   and Early Paleozoic hydrothermal activities in the Bayan Obo deposit.

326   The generation or formation of both the ore-hosting dolomite and local

327   carbonatite dykes shared similar ages ranging from 1.4 to 1.2 Ga, indicating a

328   Mesoproterozoic REE mineralization event related to carbonatite intrusion (Yang et

329   al. 2011a; Fan et al. 2014; Li et al. 2021). The subsequent Paleozoic hydrothermal

330   events had caused two significant geological processes including the subduction at

331   approximate 430 Ma or the granite intrusion at approximate 270 Ma, both of which

332   would lead to the local remobilization (Yang et al. 2011a, 2017; Campbell et al. 2014;

333   Fan et al. 2016 ; Ling et al. 2014; Liu et al. 2020). Hence, hydrothermal activity leads

334   to the reactivation of Sn and the formation of diverse Sn-rich minerals.

335   **DISCUSSION**

336   **Two different generations of cassiterite in the Bayan Obo deposit**

337   Cassiterite (SnO_2) is an essential ore mineral in Sn deposits but has not been

338   previously noted in Bayan Obo. For the first time, we report abundant cassiterite in

339   this carbonatite-hosted Fe-REE-Nb deposit and demonstrate the presence of Sn

340   mineralization. The occurrence modes of cassiterite argue for two distinctive

341   environments of crystallization.

342   In the Bayan Obo deposit, micron-sized inclusions of cassiterite are restricted

343   within massive magnetite. These two oxide minerals, cassiterite and magnetite,

344   appears to have different crystallographic affinity (tetragonal versus cubic). However,

345   their co-existence has been reported in at least two type of Sn deposits, granite-related

346   and skarn-type deposits, where the occurrence of cassiterite in magnetite has been

347   normally interpreted as an exsolution product (Wang et al. 2012, 2013). However, in

348   our present study, TEM microstructural observations provide strong evidence for the

349   simultaneous crystallization of cassiterite inclusions within the host magnetites.

350   Furthermore, magnetite forms under high-fO_2 conditions and is a sensible indicator of

351   the oxidized environment as simply known (Slack et al. 2020). On the other hand,

352   experiments demonstrated that dominates Sn in melts relative to Sn^{2+}: therefore, the

353   enrichment of Sn as cassiterite from melt also needs higher fO_2 (Bhalla et al. 2005;

354   Slack et al. 2020). This coincidence of oxidized conditions in melts may interprete the

355   intergrowth of cassiterite and magnetite in Sn deposits. As discussed above, our

356   observation could prove the co-crystallization of cassiterite with the host magnetite.

357   Columbite, Sn-bearing rutile, and monazite were also trapped in magnetite, which

358   supports a similar formation environment for magnetite and other Nb-Sn-REE

359   minerals. Yang et al. (2019) noted a similar cogenetic assemblage of magnetite with

360   hematite inclusions and suggested that the strong carbonate magmatic differentiation

361   has caused the formation of dolomite, magnetite, and significant REE accumulation in

362   the Bayan Obo deposit. Thus, it is reasonable to infer that mineral inclusions share the

363   same formation genesis with the massive magnetite that micron-, even nano-sized

364   cassiterite primarily crystallized in an early stage of carbonatite-related

365   mineralization.

366   Clustered grains of cassiterite are typically distributed in the frame of ore-hosting

367   veins. Mostly, they are observed outside of massive magnetite, indicating a later

368   formation than that of disseminated cassiterite inclusions. The Fe-rich features of

369   clustered cassiterite indicate a hydrothermal origin with relatively low forming

370   temperatures between 250 and 500 ^{o}C (Tindle and Breaks 1998a). This nature of the

371   hydrothermal environment is also supported by the intergrowth with fluorite, apatite,

372   calcite, bastnaesite, and monazite, which are considered hydrothermal minerals in the

373   Bayan Obo deposit (Liu et al. 2020; She et al. 2021).

Sn mineralization in the Bayan Obo deposit

375   In the Bayan Obo deposit, Sn enrichment is first marked by abundant cassiterite

376   inclusions in magnetite. Based on the evidence of crystallography and oxygen

377   fugacity, this study could establish a link between the early-stage Sn mineralization

378   and synchronous extensive iron mineralization during carbonatite magma evolution in

379   Bayan Obo. Interestingly, porous domains are common in massive magnetite (Fig.

380   6c). In such areas, cassiterite grains are clearly larger: this phenomenon may be linked

381   to the hydrothermal attack by fluids on magnetite, a process leading to the dissolution

382   of micron-sized cassiterite inclusions in magnetite and subsequent remobilization of

383   Sn. Successive crystallization of larger cassiterite certainly took place in this process.

384   If extensive fluid-induced fracturing occurs in magnetite during deformation, large

385   cassiterite may crystallize, even accumulate, commonly as clusters, in association

386   with fluorite, calcite, aegirine or hydrothermal amphibole, etc (Fig. 6a, d, e). Other

387   Sn-bearing minerals such as Sn-rich rutile, titanite or bafertisite, textually of

388   hydrothermal origin, have also supported the activity of Sn in hydrothermal

389   environments. The remobilization of ore-forming elements and the carbonatite-related

390   hydrothermal reaction with the country rocks have been suggested to be the driving

391   forces of REE and Nb hydrothermal mineralization in the Bayan Obo deposit, as

392   evidenced by large amounts of REE fluorocarbonates, monazite, aeschynite, and

393   pyrochlore occuring within complex mineral assemblages with fluorite, aegirine, or

394   amphibole (Liu et al. 2020; She et al. 2023). Thus, a substantial hydrothermal

395   overprinting process of Sn mineralization may be constrained.

396   The geochronological framework of the Bayan Obo deposit has been established

397   previously. As a whole, three stages can be mostly recognized, corresponding to

398   multiple magmatic and hydrothermal activities during the formation of the Bayan Obo

399   REE-Nb-Fe deposit. The original mineralization began at around 1.3 Ga, and the

400   reworking mineralization took place at 450 ~ 420 Ma as a consequence of the

401   Paleozoic magmatism (Yang et al. 2011a, 2017; Campbell et al. 2014; Fan et al.

402   2014). Younger granite of about 269 Ma (a narrow time from 263 to 281 Ma) has a

403   similar superimposed reactivation effect on the Bayan Obo district (Ling et al. 2014).

404   Indeed, the stocked Sn in magnetite can be conceived as an original Sn mineralization

405   (or enrichment), which is a part of the polymetallic mineralization during the

406   Neoproterozoic period. Our dating results of ore minerals genetically coexisting with

407   cassiterite in vein-type ores notably gave an age of 425 Ma, thus constraining an

408   Paleozoic-stage Sn mineralization, which probably has originated from the

409   reactivation of cassiterite in magnetite by the Paleozoic magmatism.

410   **Sn resources in the Bayan Obo deposit**

411   Most Sn ore deposits are associated with granite (Lehmann, 2021); by constract,

412   carbonatites are the main source of niobium and rare earth elements (Verplanck et al.

413   2016; Simandl and Paradis 2018). Although Sn may be considered an element

414   geochemically similar to niobium, its enrichment in carbonatites is uncommon, as

415   evidenced by the low Sn contents in carbonatitic rocks (several ppm, GEOROCK,

416   Appendix. Table A12) with the rare occurrence of carbonatitic cassiterite worldwide.

417   Even so, significant Sn contents may be searched out in some carbonatites. For

418   instance, the Elk Creek carbonatite in southeast Nebraska hosts the largest Nb

419   resource in the United States of America (Karl et al. 2021), which contains Sn higher

420   than 50 ppm (up to 125 ppm) in a dozen of samples (Verplanck et al. 2022). Mitchell

421   and Smith (2017) noted the "uncommon but relatively abundant" cassiterite in the

422   Ashram Zone carbonatite of the Eldor Complex (Canada); in fact, this carbonatite also

423   contains a certain amount of Sn with a weighted median of 22 ppm (Beland and

424   Williams-Jones 2021). Thus, as reported in this study, Sn enrichment and

425   mineralization in the carbonatite-related Bayan Obo deposit is not accidental but

426   merits attention on the potential importance of Sn resource in carbonatites. Based on

427   the evidence of whole-rock chemical compositions, the Bayan Obo carbonatite-related

428   deposit effectively hosts a strong Sn mineralization. The averages of bulk Sn contents

429   in banded and massive REE-Fe ores are 60 ppm, even higher than that in Sn granites

430   (usually 18 ~ 26 ppm, Lehmann, 2021). Particularly, the vein-type REE-Fe ores

431   contain 735 ppm on average, comparable with the classic threshold of Sn-mineralized

432   granites (~800 ppm, at FMQ + 3.12) (Linnen and Cuney 2005). Thus, if we earnestly

433   consider the truth of such Sn enrichment, the vein-type ores of the Bayan Obo deposit

434   and their genetic formation are worthy of continued study.

435   The Bayan Obo carbonatite-hosted deposit has immense resources of rare earth

436   elements (48 million metric tons of REEs grading 6 wt.% RE_2O_3), iron (1500 million

437   metric tons of Fe grading 35 wt.% Fe_2O_3) and niobium (2.2 million metric tons of Nb

438   grading 0.13 wt.% Nb_2O_5) (Smith et al. 2015; Fan et al. 2016). Carbonatites in Bayan

439   Obo, generally containing iron, are orebodies of rare earth elements (Fan et al. 2016).

440   As discussed above, Sn mineralization in REE-Fe ores has a close relationship with

441   Nb mineralization, thus we generally assume that the amount of Sn-bearing ores

442   corresponds to the amount of Nb-bearing ores. Therefore, we can estimate the

443   resource volume of Sn in Bayan Obo based on the Sn/Nb ratios of REE-Fe ores and

444   the known Nb resource volume of 2.2 Mt (Smith et al. 2015; Fan et al. 2016). The

445   average Sn/Nb ratios of analysed Fe-REE ores is 0.19 while the Sn/Nb ratios of vein-

446   type ores range from 0.06 to 1.09, with an average value of 0.66 according to the

447   whole-rock geochemical data. Given that the vein-type ores have the highest Sn

448   concentraion, they could be the economically important ores for Sn exploration in

449   Bayan Obo. The resource volume is equal to the quantity of ores times the grade,

450   hence we can give an rough estimation of Sn resource of 0.42 to 1.45 Mt in the Bayan

451   Obo deposit.

452   **IMPLICATIONS**

453   We have identified abundant cassiterite grains and several associated Sn-rich

454   minerals in the Bayan Obo deposit, and conclude the genetic framework of Sn

455   mineralization in this carbonatite-hosted deposit: Sn is derived from carbonatitic

456   magma, pre-enriched at around 1.3 Ga, as evidenced by the formation of dense

457   micron-sized cassiterite inclusions in massive magnetite. The subsequently Early

458   Paleozoic hydrothermal events led to the remobilization of Sn, forming larger

459   clustered cassiterite grains and Sn-rich minerals at around 425 Ma. Vein-type ores are

460   important ore-bearing rocks from Bayan Obo. Similar to Nb mineralization, Sn

461   mineralizaton in Bayan Obo probably forms a huge resource, thereby designating this

462   deposit as a prospective target for Sn mining. The potential Sn resource volume is

463   estimated to be 0.42 ~ 1.45 Mt. By studying and summarising the Sn mineralization

464   process in Bayan Obo, we can propose a possible Sn mineralization model in

465   carbonatite or carbonatite-alkaline systems. Genetically, Sn originates from deep

466   carbonate magmas and the pre-enrichment of Sn may have been the co-generation

467   between cassiterite and other dominant ore minerals of the carbonatite deposit in an

468   oxidizing environment. Subsequently hydrothermal events facilitate the reactivation

469   and precipitation of Sn, which may result in a large-scale Sn mineralization, as

470   represented by cassiterite and other Sn-bearing minerals. Our work is prospective and

471   instructive for further studies of Sn enrichment in carbonatite systems.

485   **REFERENCES CITED**

486   Beland, C.M.J., and Williams-Jones, A.E. (2021) The genesis of the Ashram REE deposit,
487   Quebec: Insights from bulk-rock geochemistry, apatite-monazite-bastnäsite
488   replacement reactions and mineral chemistry. Chemical Geology, 578, 120298.
489   Bhalla, P., Holtz, F., Linnen, R.L., and Behrens, H. (2005) Solubility of cassiterite in evolved
490   granitic melts: effect of T, fO_2, and additional volatiles. Lithos, 80, 387–400.
491   Campbell, L.S., Compston, W., Sircombe, K.N., and Wilkinson, C.C. (2014) Zircon from the
492   East Orebody of the Bayan Obo Fe–Nb–REE deposit, China, and SHRIMP ages for
493   carbonatite-related magmatism and REE mineralization events. Contributions to
494   Mineralogy and Petrology, 168, 1–23.
495   Fan, H.-R., Hu, F.-F., Yang, K.-F., Pirajno, F., Liu, X., and Wang, K.-Y. (2014) Integrated U–
496   Pb and Sm–Nd geochronology for a REE-rich carbonatite dyke at the giant Bayan Obo
497   REE deposit, Northern China. Ore Geology Reviews, 63, 510–519.
498   Fan, H.-R., Yang, K.-F., Hu, F.-F., Liu, S., and Wang, K.-Y. (2016a) The giant Bayan Obo
499   REE-Nb-Fe deposit, China: Controversy and ore genesis. Geoscience Frontiers, 7,
500   335–344.
501   ——— (2016b) The giant Bayan Obo REE-Nb-Fe deposit, China: Controversy and ore
502   genesis. Geoscience Frontiers, 7, 335–344.
503   Jochum, K.P. and Nohl, U. (2008) Reference materials in geochemistry and environmental
504   research and the GeoReM database. Chemical Geology, 253, 50-53.

505   Karl, N.A., Knudsen, L.D., and Mauk, J.L. (2021) Niobium deposits in the United States:
506   US Geological Survey data release.
507   LeBas, M.J., Keller, J., Kejie, T., Wall, F., Williams, C.T., and Peishan, Z. (1992) Carbonatite
508   dykes at bayan Obo, inner Mongolia, China. MINERALOGY AND PETROLOGY-
509   LEOBEN-, 46, 195.
510   Lehmann, B. (2021) Formation of tin ore deposits: A reassessment. Lithos, 402–403,
511   105756.
512   Ling, M.-X., Liu, Y.-L., Williams, I.S., Teng, F.-Z., Yang, X.-Y., Ding, X., Wei, G.-J., Xie,
513   L.-H., Deng, W.-F., and Sun, W.-D. (2013) Formation of the world's largest REE
514   deposit through protracted fluxing of carbonatite by subduction-derived fluids.
515   Scientific Reports, 3, 1776.
516   Ling, M.-X., Zhang, H., Li, H., Liu, Y.-L., Liu, J., Li, L.-Q., Li, C.-Y., Yang, X.-Y., and Sun,
517   W. (2014) The Permian–Triassic granitoids in Bayan Obo, North China Craton: A
518   geochemical and geochronological study. Lithos, 190, 430–439.
519   Linnen, R.L., and Cuney, M. (2005) Granite-related rare-element deposits and experimental
520   constraints on Ta-Nb-W-Sn-Zr-Hf mineralization, in Linnen RL and Samson IM, eds.,
521   rare-element geochemistry and mineral deposits. In Geological Association of Canada,
522   GAC, Short Course.
523   Li, Q.L., Li, X.H., Lan, Z.W., Guo, C.L., Yang, Y.N., Liu, Y., and Tang, G.Q. (2013)
524   Monazite and xenotime U–Th–Pb geochronology by ion microprobe: dating highly
525   fractionated granites at Xihuashan tungsten mine, SE China. Contributions to
526   Mineralogy and Petrology, 166, 65–80.
527   Li, Q.-L., Huyskens, M.H., Yang, Y.-H., Ling, X.-X., Yin, Q.-Z., Nikiforov, A. V, and Li, X.-
528   H. (2020) Bastnaesite K-9: A homogenous natural reference material for in-situ U-Pb
529   and Th-Pb dating. Atomic Spectroscopy, 41, 218–222.
530   Liu, S., Fan, H.-R., Groves, D.I., Yang, K.-F., Yang, Z.-F., and Wang, Q.-W. (2020)
531   Multiphase carbonatite-related magmatic and metasomatic processes in the genesis of
532   the ore-hosting dolomite in the giant Bayan Obo REE-Nb-Fe deposit. Lithos, 354,
533   105359.
534   Li, X.-C., Fan, H.-R., Zeng, X., Yang, K.-F., Yang, Z.-F., Wang, Q.-W., and Li, H.-T. (2021)
535   Identification of~ 1.3 Ga hydrothermal zircon from the giant Bayan Obo REE deposit
536   (China): Implication for dating geologically complicated REE ore system. Ore
537   Geology Reviews, 138, 104405.
538   Mitchell, R.H., and Smith, D.L. (2017) Geology and mineralogy of the Ashram Zone
539   carbonatite, Eldor Complex, Québec. Ore Geology Reviews, 86, 784–806.
540   She, H.-D., Fan, H.-R., Yang, K.-F., Li, X.-C., Yang, Z.-F., Wang, Q.-W., Zhang, L.-F., and
541   Wang, Z.-J. (2021) Complex, multi-stage mineralization processes in the giant Bayan
542   Obo REE-Nb-Fe deposit, China. Ore Geology Reviews, 139, 104461.
543   She, H.-D., Fan, H.-R., Santosh, M., Li, X.-C., Yang, K.-F., Wang, Q.-W., Wei, W., Liu, Y.-J.,
544   Liu, S., and Liu, S.-L. (2023) Paleozoic remelting of carbonatite in Bayan Obo
545   (China): Further insights into the formation of a giant REE deposit. Gondwana
546   Research, 119, 172–185.

547 Simandl, G.J., and Paradis, S. (2018) Carbonatites: related ore deposits, resources, footprint,
548   and exploration methods. Applied Earth Science, 127, 123–152.

549 Slack, J.F., Neymark, L.A., Moscati, R.J., Lowers, H.A., Ransom, P.W., Hauser, R.L., and
550   Adams, D.T. (2020) Origin of Tin Mineralization in the Sullivan Pb-Zn-Ag Deposit,
551   British Columbia: Constraints from Textures, Geochemistry, and LA-ICP-MS U-Pb
552   Geochronology of Cassiterite. Economic Geology, 115, 1699–1724.

553 Smith, M.P., Campbell, L.S., and Kynicky, J. (2015) A review of the genesis of the world
554   class Bayan Obo Fe–REE–Nb deposits, Inner Mongolia, China: Multistage processes
555   and outstanding questions. Ore Geology Reviews, 64, 459–476.

556 Song, W., Xu, C., Smith, M.P., Chakhmouradian, A.R., Brenna, M., Kynický, J., Chen, W.,
557   Yang, Y., Deng, M., and Tang, H. (2018) Genesis of the world's largest rare earth
558   element deposit, Bayan Obo, China: Protracted mineralization evolution over~ 1 by.
559   Geology, 46, 323–326.

560 Tindle, A.G., and Breaks, F.W. (1998a) Oxide minerals of the separation rapids rare-element
561   granitic pegmatite group, northwestern Ontario. The Canadian Mineralogist, 36, 609–
562   635.

563 ——— (1998b) Oxide minerals of the Separation Rapids rare-element granitic pegmatite
564   group, northwestern Ontario. The Canadian Mineralogist, 36, 609–635.

565 Verplanck, P.L., Mariano, A.N., and Mariano, A. (2016) Rare earth element ore geology of
566   carbonatites.

567 Verplanck, P.L., Lang Farmer, G., Kettler, R.M., Lowers, H.A., Johnson, C.A., Koenig, A.E.,
568   and Blessington, M.J. (2022) Petrogenesis and rare earth element mineralization of the
569   Elk Creek carbonatite, Nebraska, USA. Ore Geology Reviews, 146, 104953.

570 Wang, R.C., Yu, A.-P., Chen, J., Xie, L., Lu, J.-J., and Zhu, J.-C. (2012) Cassiterite
571   exsolution with ilmenite lamellae in magnetite from the Huashan metaluminous tin
572   granite in southern China. Mineralogy and Petrology, 105, 71–84.

573 Wang, R.C., Xie, L., Chen, J., Yu, A., Wang, L., Lu, J., and Zhu, J. (2013) Tin-carrier
574   minerals in metaluminous granites of the western Nanling Range (southern China):
575   Constraints on processes of tin mineralization in oxidized granites. Journal of Asian
576   Earth Sciences, 74, 361–372.

577 Yang, K., Fan, H., Pirajno, F., and Li, X. (2019) The Bayan Obo (China) giant REE
578   accumulation conundrum elucidated by intense magmatic differentiation of
579   carbonatite. Geology, 47, 1198–1202.

580 Yang, K.-F., Fan, H.-R., Santosh, M., Hu, F.-F., and Wang, K.-Y. (2011a) Mesoproterozoic
581   carbonatitic magmatism in the Bayan Obo deposit, Inner Mongolia, North China:
582   Constraints for the mechanism of super accumulation of rare earth elements. Ore
583   Geology Reviews, 40, 122–131.

584 ——— (2011b) Mesoproterozoic mafic and carbonatitic dykes from the northern margin of
585   the North China Craton: implications for the final breakup of Columbia
586   supercontinent. Tectonophysics, 498, 1–10.

587 Yang, X., Lai, X., Pirajno, F., Liu, Y., Mingxing, L., and Sun, W. (2017) Genesis of the
588   Bayan Obo Fe-REE-Nb formation in Inner Mongolia, north China craton: a

589   perspective review. Precambrian Research, 288, 39–71.

590   Zhang, S.-H., Zhao, Y., and Liu, Y. (2017) A precise zircon Th-Pb age of carbonatite sills

591   from the world's largest Bayan Obo deposit: Implications for timing and genesis of

592   REE-Nb mineralization. Precambrian Research, 291, 202–219.

593   Zhu, X., Sun, J., and Pan, C. (2015) Sm–Nd isotopic constraints on rare-earth mineralization

594   in the Bayan Obo ore deposit, Inner Mongolia, China. Ore Geology Reviews, 64, 543–

595   553.

596

597

598 Table 1. Tin contents of different types of ores (ICP-MS analyses)

| 599 Ore type	Main mineral assemblages	Sn contents (ppm)		Nb contents (ppm)		Sc contents (ppm)		La contents (ppm)	
Disseminated	Dolomite+fluorite (DK2006)	9.04	Average	356.07	Average	56.26	Average	5259.68	Average
	Dolomite (DK2012)	10.00	(15.03)	80.60	(677.80)	26.60	(43.92)	9220.00	(4594.30)
	Dolomite+fluorite (DK1904)	11.67		170.63		19.70		2434.09	
	Dolomite (XK1922)	17.45		2279.68		41.92		4557.72	
	Dolomite+fluorite (XK2035)	27.00		502.00		75.10		1500.00	
Banded	Magnetite+fluorite+REE minerals (ZK1917)	44.52	Average	1922.62	Average	113.95	Average	3233.93	Average
	Phlogopite+magnetite+REE minerals (17BY39)	151.00	(61.92)	1845.00	(945.62)	80.80	(73.29)	1165.00	(>5758.15)
	Fluorite+aegirine+magnetite (DK1901)	15.00		57.10		13.60		>10000	
	Fluorite+aegirine+magnetite (DK1903)	29.00		546.00		72.50		7170.00	
	Fluorite+magnetite+aegirine (DK2004)	119.00		758.00		91.60		>10000	
	Fluorite+dolomite (XK2037)	13.00		545.00		67.30		2980.00	
Massive	Magnetite+dolomite (17BY16)	23.16	Average	972.35	Average	28.16	Average	1475.52	Average
	Magnetite+Fluorite (17BY158)	34.56	(62.42)	645.25	(717.64)	116.15	(53.95)	277.28	(>3801.15)
	Aegirine+magnetite (17BY62)	42.00		267.00		42.50		>10000	
	Magnetite+aegirine (ZK1932)	36.00		297.00		31.50		518.00	
	Fluorite+magnetite (DK1909)	17.00		340.00		17.80		>10000	
	Magnetite+fluorite/calcite/aegirine/Na-amphibole (ZK1918)	200.21		871.90		51.12		3167.26	
	Magnetite+fluorite/calcite/aegirine/Na-amphibole (ZK1919)	/		/		/		/	
	Fluorite+magnetite+calcite (XK2028)	84.00		1630.00		90.40		1170.00	
Vein-type	Aegirine+magnetite (DK1906)	256.91	Aeverage	4407.34	Average	164.46	Average	2370.91	Average
	Aegirine+fluorite+bafertisite (DK2003)	1515.00	(735.23)	1650.00	(1857.84)	108.50	(93.77)	7090.00	(>5820.23)
	Aegirine+Na-amphibole+bafertisite (DK2007)	794.00		759.00		49.40		3820.00	
	Aegirine (DK2022)	375.00		615.00		52.70		>10000	
All samples			Average (173.84)		Average (978.07)		Average (64.18)		Average (>4882.25)

600

Table 2. Representative electron-microprobe results of clustered cassiterite in from vein-type ores

No.	Cassiterite associated with fluorite (n=17)						Cassiterite associated with aegirine (n=11)					
	1	2	3	Min	Max	Ave.	1	2	3	Min	Max	Ave.
TiO_2	0.57	0.27	0.28	0.06	0.57	0.30	2.48	3.15	2.62	2.17	6.07	3.32
CaO	0.59	1.07	0.82	0.57	1.07	0.76	0.65	0.55	0.50	0.50	1.02	0.60
SnO_2	97.42	97.30	98.55	95.91	99.53	97.93	93.86	92.65	93.81	89.17	95.74	93.29
SiO_2	0.16	0.24	0.19	0.14	1.55	0.35	0.61	0.31	1.37	0.18	1.40	0.47
Ta_2O_5	0.00	0.00	0.00	0.00	0.05	0.01	0.00	0.00	0.07	0.00	0.07	0.01
FeO	0.89	0.17	0.28	0.05	1.01	0.41	1.94	2.26	1.14	1.11	2.37	1.61
MnO	0.04	0.02	0.00	0.00	0.05	0.01	0.34	0.42	0.12	0.12	0.49	0.25
Nb_2O_5	0.08	0.08	0.10	0.00	0.59	0.13	0.19	0.95	0.23	0.19	1.11	0.49
MgO	0.12	0.22	0.12	0.08	0.22	0.11	0.12	0.12	0.08	0.07	0.13	0.10
Total	99.88	99.36	100.34	98.21	100.72	100.00	100.19	100.40	99.93	99.00	101.09	100.13
a.p.f.u based on O=2												
Ti	0.01	0.01	0.01	0.00	0.01	0.01	0.05	0.06	0.05	0.04	0.11	0.06
Ca	0.02	0.03	0.02	0.02	0.03	0.02	0.02	0.01	0.01	0.01	0.03	0.02
Sn	0.96	0.97	0.97	0.94	0.98	0.97	0.90	0.89	0.90	0.84	0.93	0.89
Si	0.00	0.01	0.00	0.00	0.04	0.01	0.01	0.01	0.03	0.00	0.03	0.01
Ta	0.00	0.00	0.00	0.00	0.00	0.00	0.00	0.00	0.00	0.00	0.00	0.00
Fe	0.02	0.00	0.01	0.00	0.02	0.01	0.04	0.05	0.02	0.02	0.05	0.03
Mn	0.00	0.00	0.00	0.00	0.00	0.00	0.01	0.01	0.00	0.00	0.01	0.01
Nb	0.00	0.00	0.00	0.00	0.01	0.00	0.00	0.01	0.00	0.00	0.01	0.01
Mg	0.00	0.01	0.00	0.00	0.01	0.00	0.00	0.00	0.00	0.00	0.00	0.00
Total	1.02	1.02	1.02	1.01	1.02	1.02	1.03	1.03	1.02	1.02	1.04	1.03
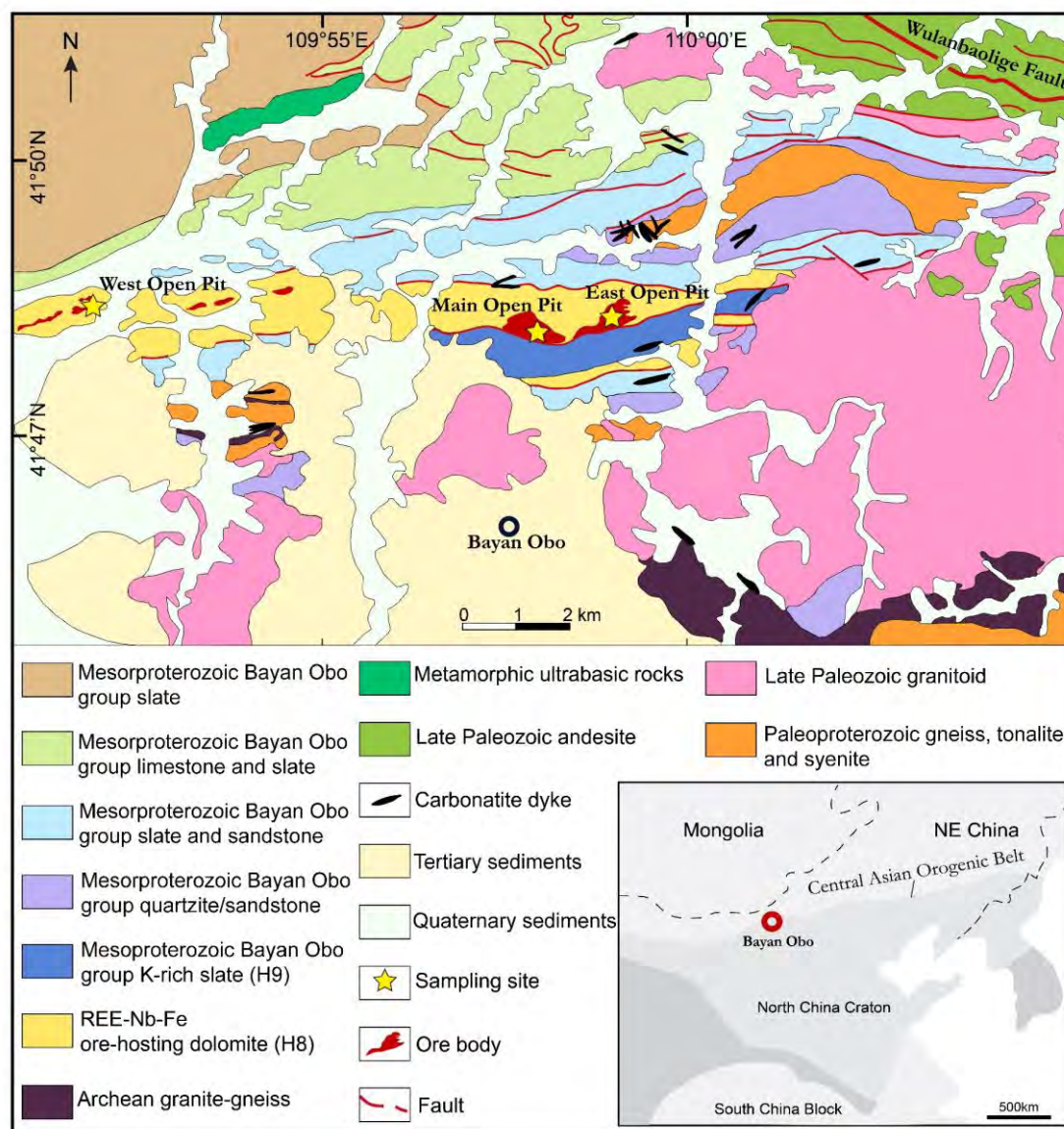
601
602   **FIGURE 1.** Geological map of the Bayan Obo region modified after Fan et al.
603   (2016). Inset tectonic map showing the location of the Bayan Obo deposit at the
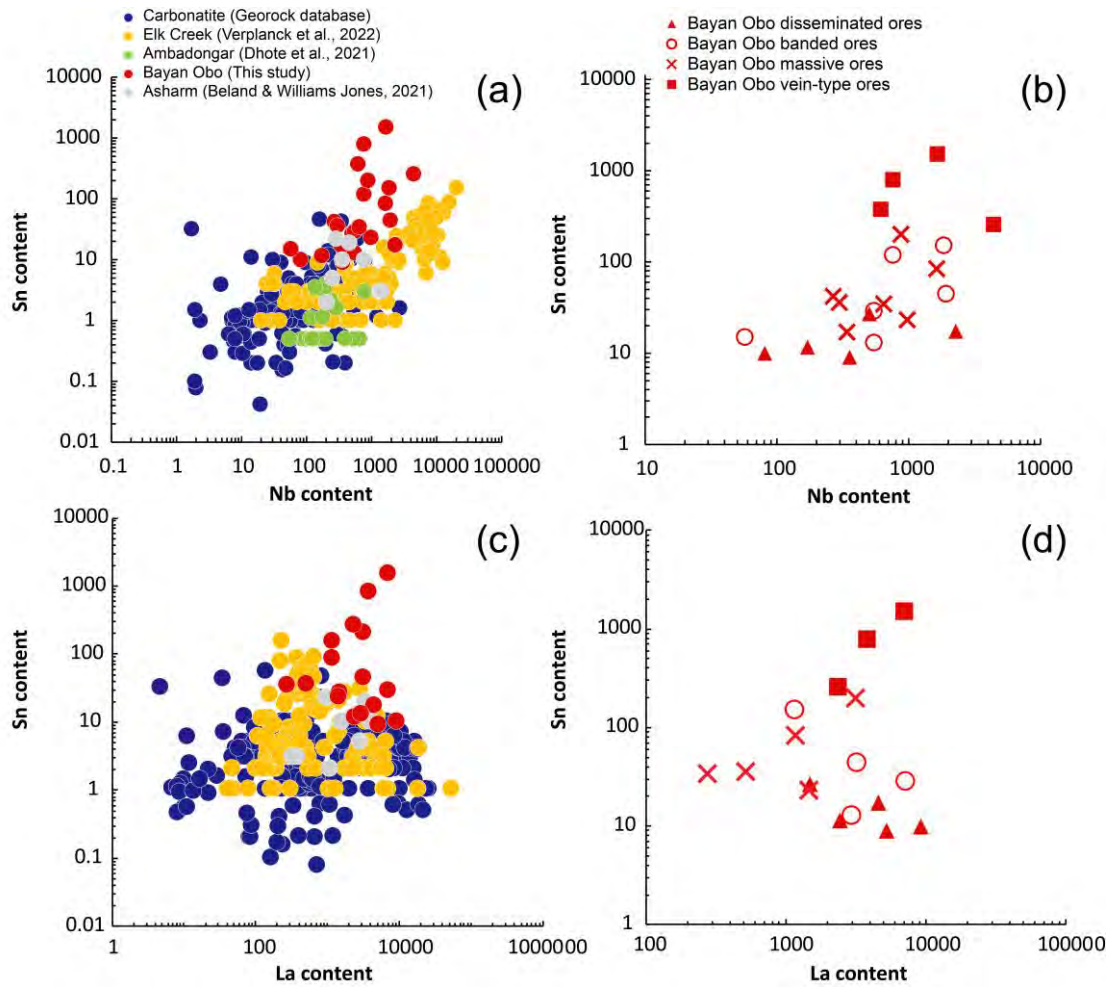604   northern margin of the North China Craton, adapted from Ling et al. (2013).
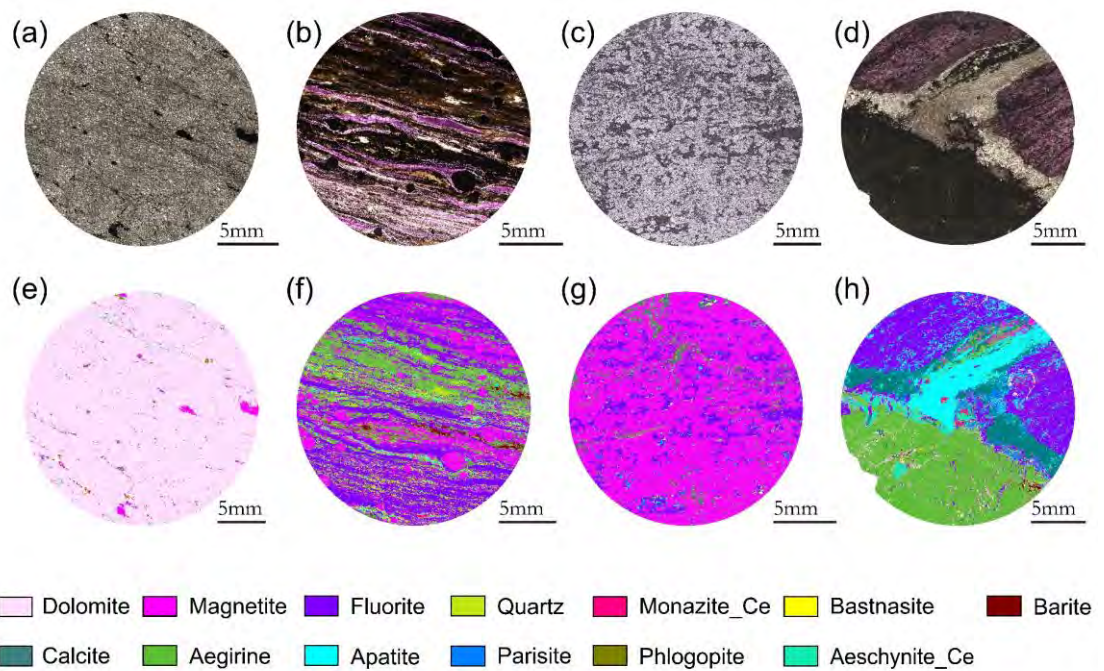
FIGURE 2. Single polarized microscope images and AMICS (Advanced Mineral Identification and Characterization System) images illustrating ore textures and mineral assemblages of REE-Fe ores in the Bayan Obo deposit. (a, e) disseminated ore; (c, g) banded ore; (b, f) massive ore; (d, h) vein-type ore.

FIGURE 3. Binary plots (logarithmic scales) of Nb content vs. Sn content (a, b) and La content vs. Sn content (c, d) in bulk from Bayan Obo deposit and other carbonatites.

614
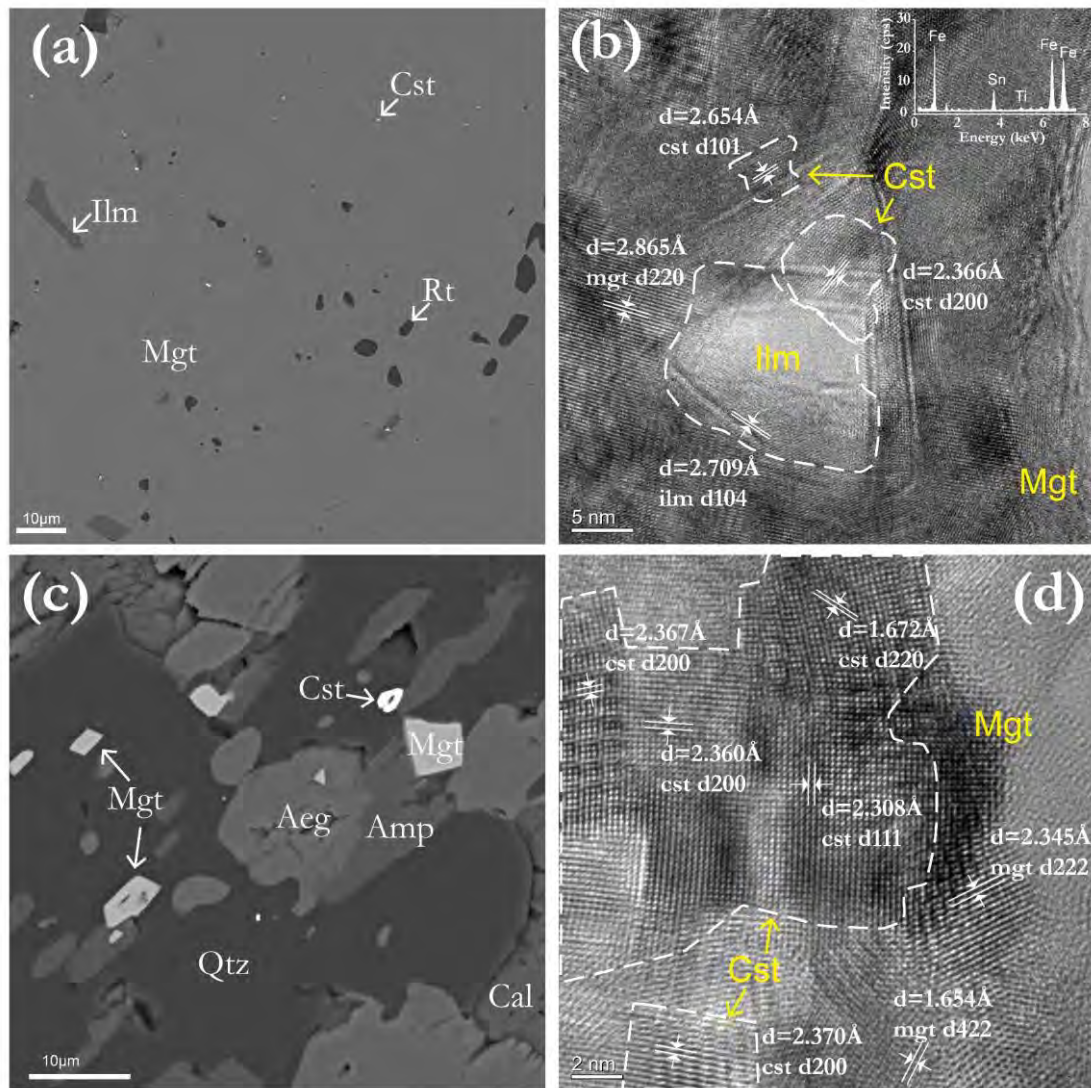
615   **FIGURE 4.** BSE (a, c) and TEM images (b, c) of magnetite grains associated
616   with cassiterite.

617
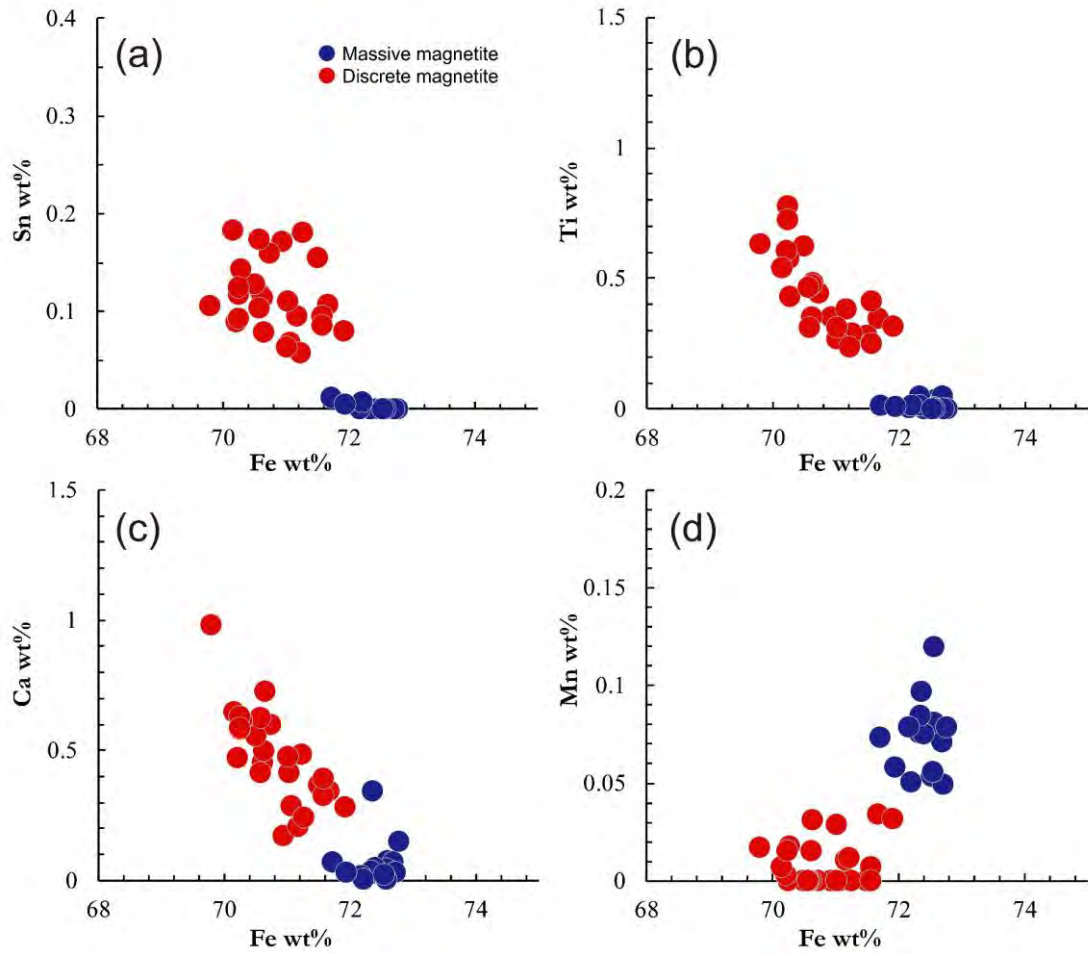
618   **FIGURE 5.** Binary plots of Fe vs. Sn (a), Fe vs. Ti (b), Fe vs. Ca (c) and Fe vs.
619   Mn (d) to distinguish massive magenetite and discrete magnetite in the Bayan
620   Obo deposit.
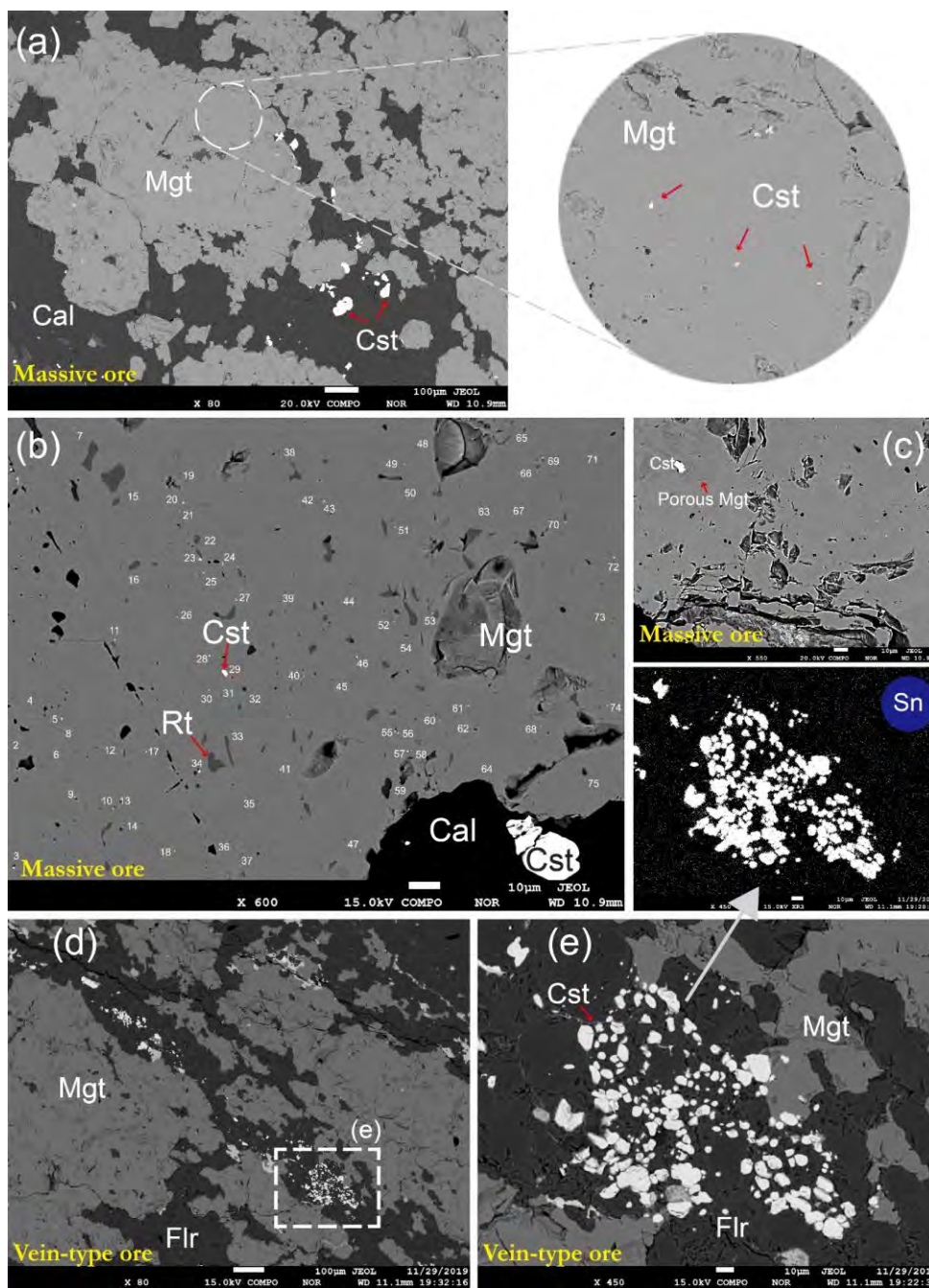
FIGURE 6. Scanning electron microscope investigation of cassiterite in the Bayan Obo deposit. (a) Disseminated cassiterite inclusions in massive magnetite. The inset enlargement shows the micron-sized grains of cassiterite (arrowed). Note that larger cassiterite grains tens of microns across occurs in the calcite vein outside of magnetite. (b) Abundance of micro-inclusions of disseminated cassiterite grains within massive magnetite (numbers alongside 75 grains of cassiterite identified with Sn X-ray scanning); Sn-bearing rutile is also arrowed. (c) Porous domain with one larger cassiterite grain (upper left) in magnetite. Micron-sized cassiterite inclusions are also indicated by arrow for comparison. (d, e) Clustered cassiterite in fluorite surrounding or cutting magnetite. Abbreviation: Cst = cassiterite; Mgt = magnetite; Cal = calcite; Rt = rutile; Flr =

633   fluorite.
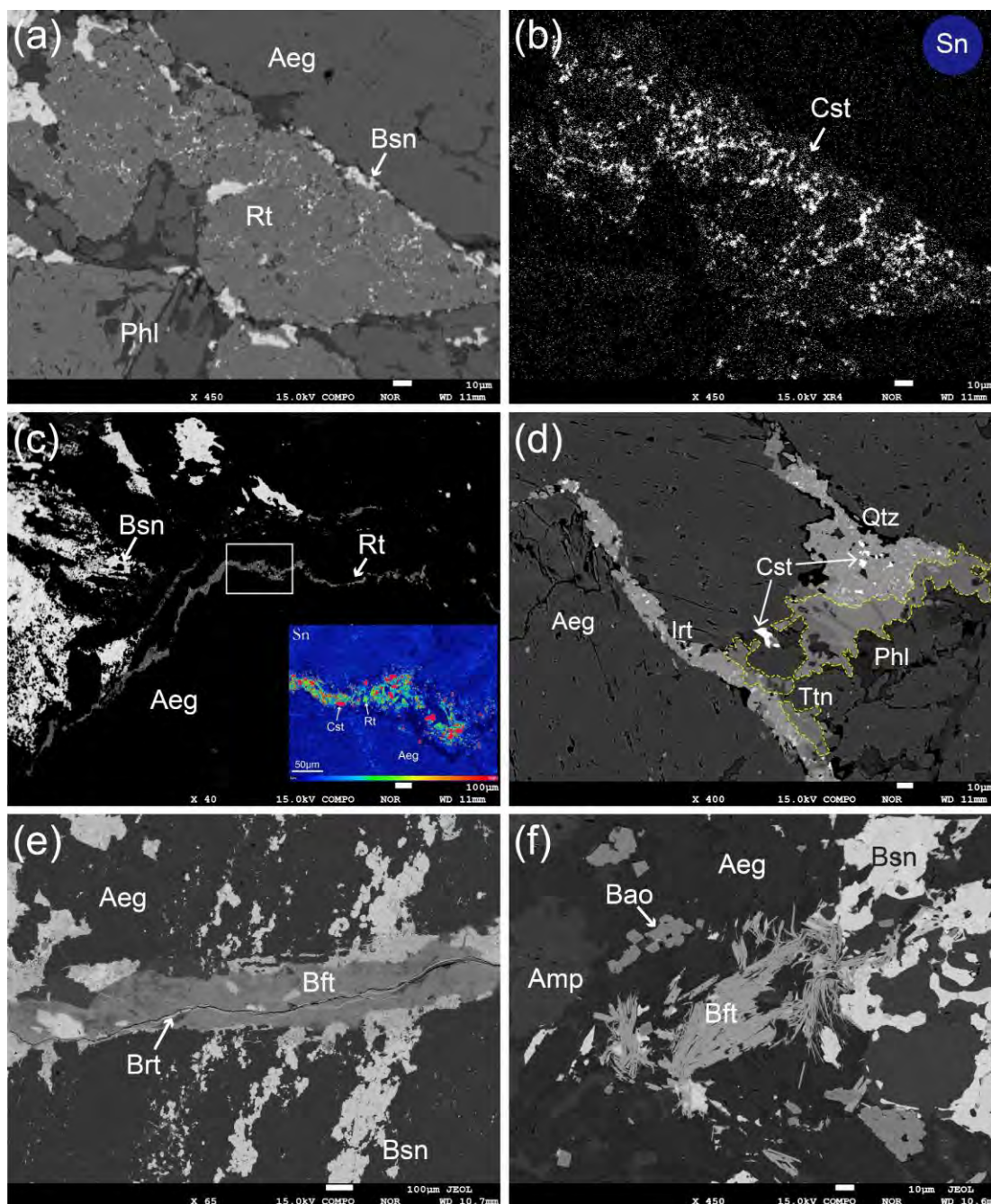
FIGURE 7. Scanning electron microscope investigation of other Sn-bearing minerals in the Bayan Obo deposit. (a) BSE and Sn X-ray scanning mapping of cassiterite accumulating with aggregates of subhedral Sn-rich rutile. (b) Same area in (a) showing occurrence of cassiterite with rutile (Sn scanning image). (c) Veinlets of rutile crosscutting the aegirine (BSE image). (d) BSE image of Sc-rich titanite in vein-type ore (e) Veinlet of Sn-bearing bafertisite (BSE image). (f) Aggregates of fiber Sn-rich bafertisite (BSE image). Aeg = aegirine; Amp = amphibole; Bao= baotite; Bft = bafertisite; Brt = baryte; Bsn = bastnaesite; Cst = cassiterite; Irt = ilmenorutile; Phl = phlogopite; Qtz = quartz; Rt = rutile; Ttn = titanite.
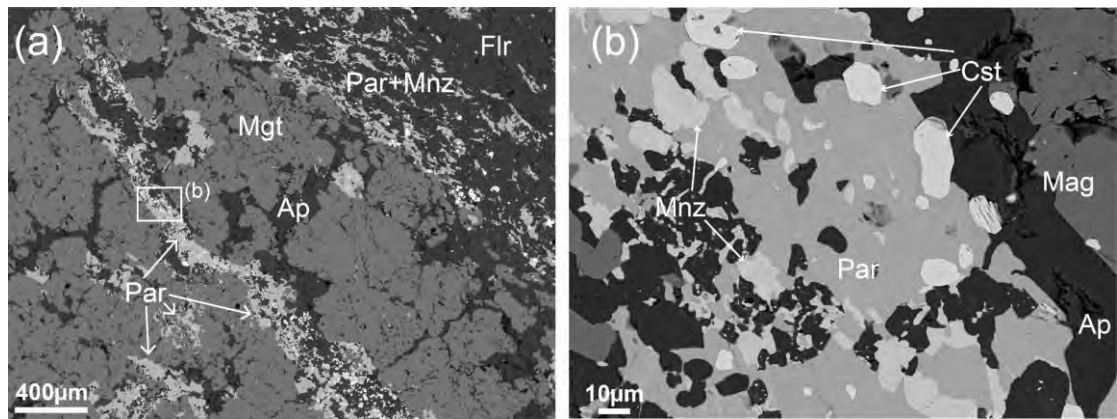
645
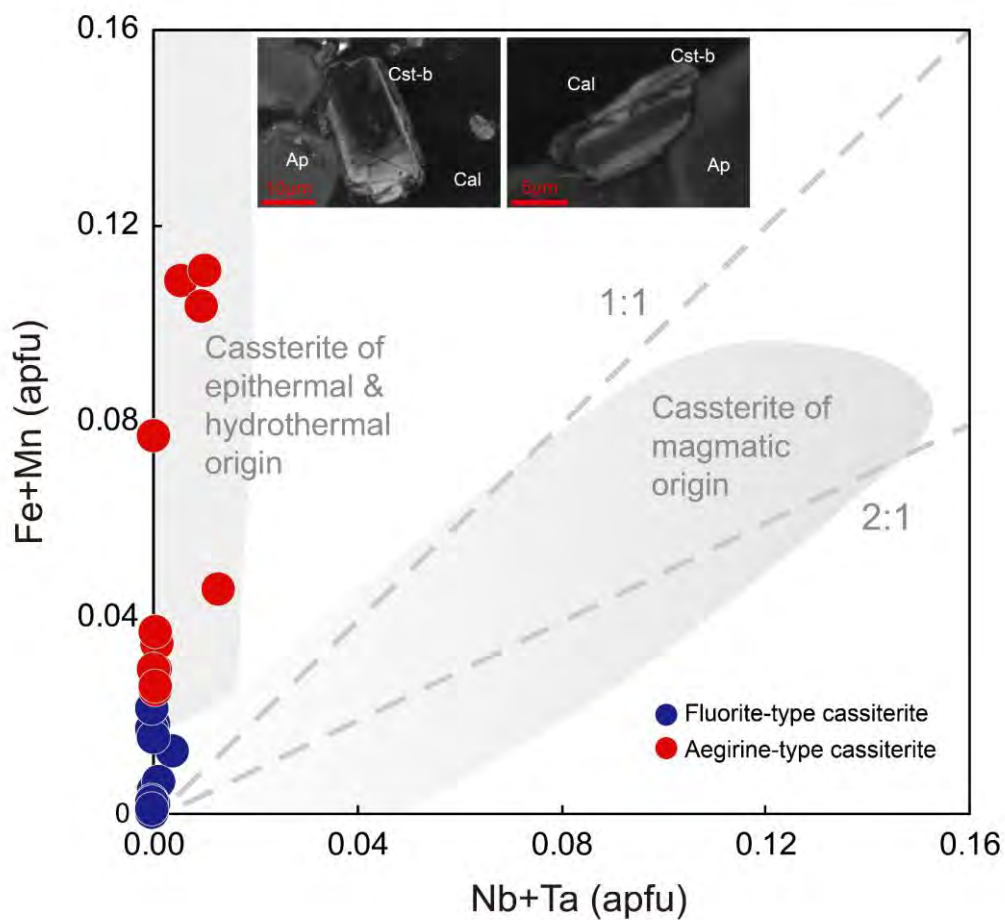
FIGURE 8. (Nb+Ta) vs (Fe+Mn) diagram for clustered cassiterite (EPMA data). Shaded areas indicate cassiterite of magmatic or hydrothermal origin (modified after Tindle & Breaks, 1998). Inset CL images show zonation of representative analyzed cassiterite grains. Cst = cassiterite; Ap = apatite; Cal = calcite.
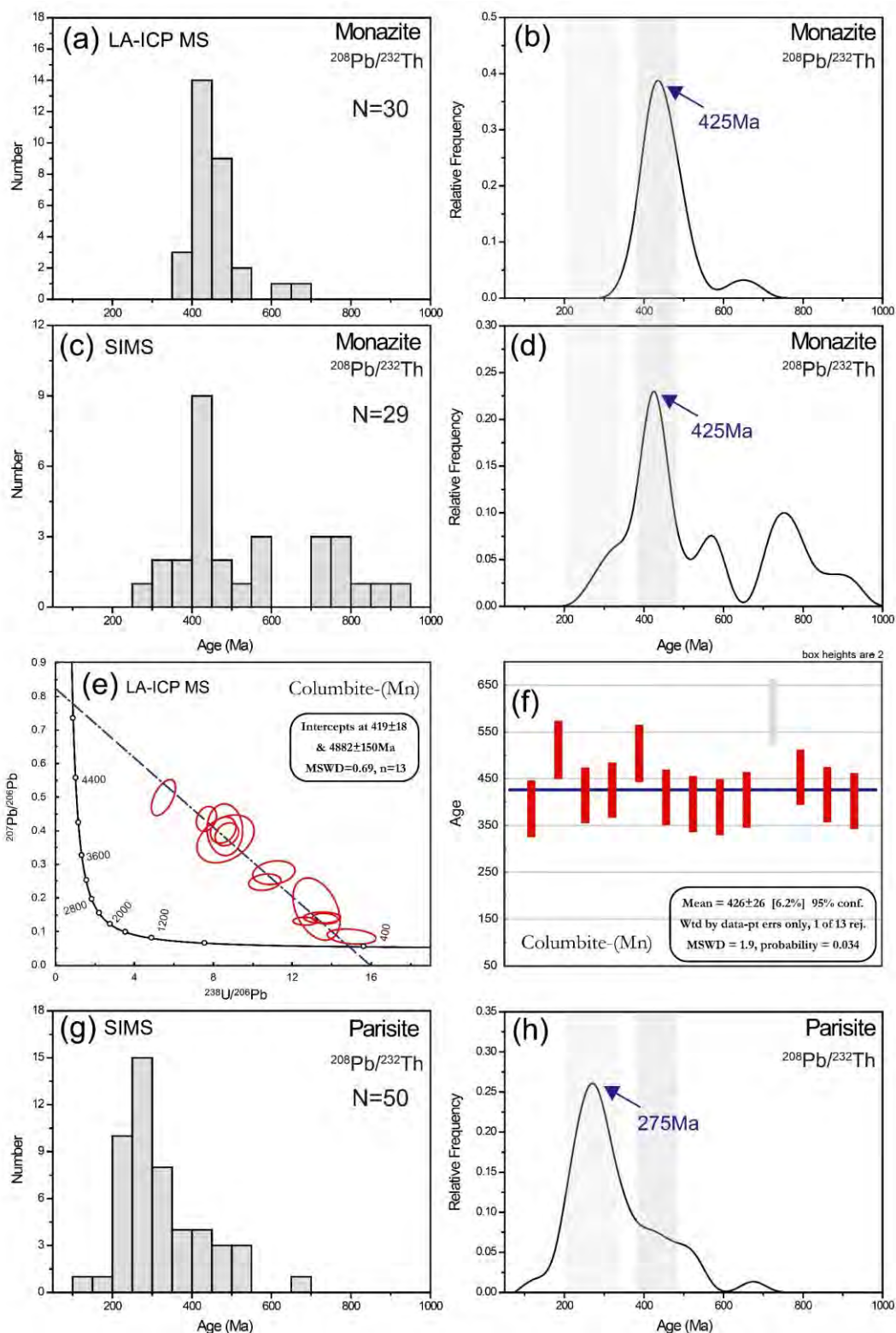
650

FIGURE 9. The backscattered electron (BSE) images of monazite and parisite co-existing with cassiterite in the vein-type ore from the Bayan Obo deposit.

653

FIGURE 10. *In-situ* U-Th-Pb dating of ore minerals coexisting with cassiterite.
(a, b) Frequency distribution histogram and relative probability plots of monazite
LA-ICP-MS ages; (c, d) Frequency distribution histogram and relative
probability plots of monazite SIMS ages; (e, f) Columbite LA ICPMS ages; (f, g)

658   Frequency distribution histogram and relative probability plots of parisite SIMS
659   ages.